Harmonic Image Reconstruction Assisted by a Nonlinear Metmaterial Surface

Zhiyu Wang,[1] Yu Luo,[1,3] Tao Jiang,[1] Zheng Wang,[2,*] Jiangtao Huangfu,[1,†] and Lixin Ran[1,‡]

[1]*Department of Information and Electronic Engineering, Zhejiang University, Hangzhou 310027, China*
[2]*Department of Physics, Massachusetts Institute of Technology, Cambridge, Massachusetts 02139, USA*
[3]*The Blackett Laboratory, Department of Physics, Imperial College London, London SW7 2AZ, UK*

(Received 19 August 2010; published 25 January 2011)

We experimentally demonstrate a microwave far-field image reconstruction modality with the transverse resolution exceeding the diffraction limit by using a single layer of highly nonlinear metamaterial. The harmonic fields of the nonlinear metamaterial surface allow the far-field propagation of wave fronts with spatial frequencies several times higher than that of the fundamental field. Near-field images can thus be mathematically recovered from the far-field patterns of the harmonic fields.

DOI: 10.1103/PhysRevLett.106.047402 PACS numbers: 78.67.Pt, 42.70.Mp, 84.40.−x

In linear media, the spatial resolution of an electromagnetic imaging system has long been considered to be limited by the Rayleigh limit, approximately at one half of the wavelength [1]. Recent studies in left-handed metamaterials and nonlinear microscopy have resulted in several super-resolution schemes that promise subwavelength imaging. Using only linear media, artificial left-handed metamaterials have been proposed [2] and experimentally verified [3–5] to restore the evanescent waves that carry subwavelength spatial information in near-field and far-field configurations. Metamaterials, such as "hyper lenses," have been show to transform evanescent waves into propagating waves for reconstructing subwavelength features in the far field [6–9]. Nevertheless linear metamaterials are intrinsically lossy, which necessitates a trade-off between the improved spatial resolution and the reduced signal-to-noise ratio of the transmitted images. Metamaterials built from gain medium represent one approach to compensate for the absorption loss [10]. On the other hand, nonlinear optical schemes such as harmonic optical microscopy [11] and nonlinear fluorescence microscopy [12] have also been developed to capture spatial details finer than the diffraction limit without sacrificing the signal-to-noise ratio. However, these nonlinear optical schemes are restricted to operate at visible and near infrared wavelengths, where naturally occurring transparent nonlinear media are abundant. In this Letter, we propose and demonstrate experimentally that a diode-based nonlinear metamaterial surface that features an artificial nonlinearity is not limited to a particular wavelength. More importantly, when placed in the near field of the object, the metamaterial surface generates harmonic fields that allow for far-field imaging of details at a resolution far beyond the diffraction limit of the fundamental frequency.

Harmonic imaging, widely used in both optical microscopy [11] and ultrasonic imaging [13], relies on the enhanced spatial resolution of frequency harmonics generated in a nonlinear medium. For instance, when compared to the fundamental frequency of the incidence radiation, the second harmonic features a wavelength 50% shorter and permits far-field propagation of spatial patterns with a doubled resolution. The illumination at the fundamental frequency is converted into high-order harmonics by the nonlinear sample, which is subsequently captured by a far-field image reconstruction system. A conventional harmonic imaging system relies on the intrinsic nonlinearity of the sample being probed, while using metamaterials allows the introduction of artificial nonlinearity to a sample without being subject to the associated restrictions on wavelengths and crystalline symmetry [14]. A concrete example of such a scenario is illustrated in Fig. 1 and will be experimentally examined in this Letter. We consider a sample composed of two linear antennas in free space, radiating in phase and placed at a distance $d = 0.5\lambda$, where λ is the free-space wavelength of the driving frequency f_0. Since their distance d is smaller than the diffraction limit for two in-phase point sources [1], the two antennas cannot be resolved from their far-field radiation pattern. The evanescent waves carrying the subwavelength spatial distribution of the sources decay

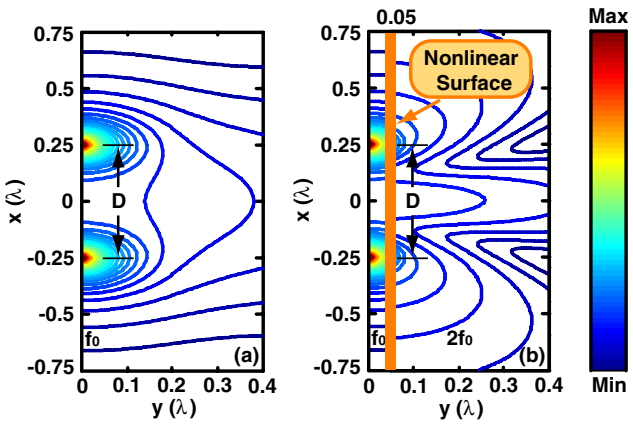

FIG. 1 (color online). Calculated near-field intensity distribution of two in-phase dipole sources (a) at the source frequency f_0, and (b) at frequency $2f_0$.

rapidly in the far field. The calculated intensity distribution [Fig. 1(a)] indicates that, even in the near field, the two dipoles can only be distinguished in their immediate vicinity, an area within 0.2λ from the sources known as the "reactive zone" or "reactive near-field region" [15]. In contrast, these two dipoles can be distinguished, even in the far field, at the second and the higher-order harmonic frequencies, because their distance is now equal to or greater than the free-space wavelengths of the harmonics, well above the diffraction limit. The calculated intensity distribution for the second harmonic, for example, is shown Fig. 1(b). Here, the key to generate the harmonic radiations without resorting to the intrinsic nonlinearity of the sample is the placement of a highly nonlinear metamaterial surface within the reactive zone where the evanescent field at the fundamental frequency dominates. The subfundamental-wavelength spatial information carried in the evanescent waves is then converted into the second and higher order harmonics that can be detected in the far field with conventional imaging systems.

Many nonlinear metamaterial designs have been proposed and realized using active circuit elements. One of the first nonlinear electromagnetic metamaterials was proposed by Pendry *et al.* [16] and have been realized in Refs. [17–20]. Among many implementations, diode-based metamaterials have been demonstrated to exhibit strong nonlinearity under low incident power [21–24]. In this Letter, we use the nonlinear metamaterial design reported in an earlier publication [25], shown in the right inset of Fig. 2(a). The metamaterial consists of two layers of two-dimensional arrays of I-shaped metallic traces printed and aligned on both sides of a 1 mm-thick FR4 substrate with a relative permittivity of 4.6. In each unit cell, a small gap in the center of the I pattern holds a microwave diode (Infineon's BAT15-03W) electrically in contact with the metallic traces [top-right inset of Fig. 2(a)]. The diodes are biased at 0.9 V (dc), corresponding to a highly nonlinear region of their current-voltage characteristic. The dimensions of the metallic traces in each unit cell are $l = h = 6$ mm, $g = 1.6$ mm, $w_1 = 0.3$ mm, $w_2 = 1$ mm. The entire metamaterial structure spans 40 unit cells along the x direction and 48 unit cells along the z directions, yielding a 288 mm-long, 240 mm-wide, 1 mm-thick thin sheet. For incident waves with the electric fields polarized along the z direction, electric resonances are induced by the metallic resonant patterns and produce driving currents across the diodes. Because of the highly nonlinear I-V characteristics of the diodes, the currents contain large harmonic components of the fundamental frequency and reradiate into the free space through the metallic patterns [25].

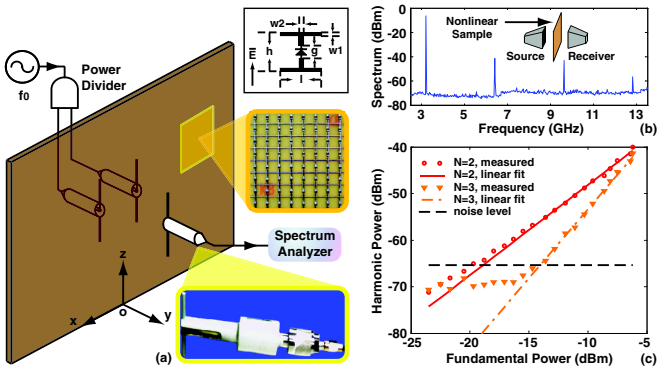

FIG. 2 (color online). (a) Schematic of the experiment setup for harmonic image reconstruction. (b) Measured power spectrum of harmonic components generated from the nonlinear surface using a plane-wave setup. (c) Measured power dependence (markers) of the harmonic components agrees well with an effective nonlinearity model (curves) [26].

The effective nonlinear coefficients of the metamaterial surface are measured in a free-space transmission setup, shown in Fig. 2(b). An incident monochromatic wave at 3.2 GHz with an approximate plane-wave wave front illuminates the sample from the left. The generated harmonic waves are measured on the right side by another wide-band horn antenna. Spectral analysis of the received signal reveals that the second, third, and forth order harmonics at 6.4, 9.6, and 12.8 GHz are excited with high signal-noise ratios at an incident power level 5.7 dBm. Since the free-space wavelength (100 mm) of the fundamental frequency far exceeds the 6 mm period of the unit cells, the sample can be regarded as a thin sheet of effective medium at fundamental and lower order harmonic frequencies. In order to extract the effective nonlinear coefficient, we measure the power level of the second and the third harmonics with the incident power swept from -14 to 7 dBm, as shown in Fig. 2(c). For a uniform sheet of nonlinear material in the nondepletion regime, the power I_N of the generated Nth harmonic can be analytically related to the fundamental power I_1 of the fundamental as follows [14]:

$$I_N = \frac{\omega_N^2 I_1^N}{2^{N+1} n_1^N n_N \varepsilon_0^{N-1} c^{N+1}} \left[\chi_{\text{eff}}^{(N)} L\right]^2, \qquad N = 2, 3 \qquad (1)$$

where ω_N is the angular frequency of the Nth harmonic as $\omega_N = N\omega_1$. n_N denotes the refractive index for the Nth harmonic. We notice that the power of the Nth harmonic is dependent on the thickness of the sample as it grows quadratically with the product of the nonlinear susceptibility $\chi_{\text{eff}}^{(N)}$ and the thickness of the nonlinear surface L. Therefore, using the product of $\chi_{\text{eff}}^{(N)} L$ as a normalized effective nonlinear coefficient allows us to treat the nonlinear metamaterial surface without an explicit consideration of the thickness. Furthermore, taking into account of the large reflection at the surfaces of the nonlinear metamaterial that reduces the transmitted fundamental power from the incident power by 10 dB, the fundamental power I_1 is taken from the transmitted power in agreement with the nondepletion approximation. Excellent agreement between the measurement and the effective nonlinear

medium treatment can be seen in Fig. 2(c), as the measured power of the second harmonic and the third harmonic indeed grow to the second and the third power of the fundamental, respectively (see a detailed analysis in the supplemental material [26]). The metamaterial sample can thus be treated as a nonlinear effective medium.

With the strong nonlinearity established in the metamaterial sample, we test its effectiveness in harmonic image reconstruction of spatial features beyond the diffraction limit of the fundamental wavelength. The scenario discussed earlier in Fig. 1 is recreated using an experimental setup depicted in Fig. 2(a). Two standard dipole antennas, serving as sources in the vicinity of the metamaterial surface, are polarized along the z direction and driven with identical amplitude and phase at 3 GHz and 20 dBm by a Vector Signal Generator (Agilent E8267C). A third identical dipole antenna serves as a detector on the other side of the metamaterial sample and is spatially scanned to map the field amplitude through a Spectrum Analyzer (Advantest R3271A). The near-field mapping is conducted in a microwave anechoic chamber, where we move the third dipole antenna along the x axis at four different distances, i.e., $y = 10$, 20, 30, and 40 mm, respectively. In addition, the far-field radiation pattern is measured using a broadband horn antenna 600 mm away from the sources, with the source antennas and the nonlinear metamaterial sample rotated in the quiet zone of the chamber.

We start the measurement with the two source antennas placed 50 mm apart, well below the diffraction limit for two in-phase point sources [1]. In a controlled experiment where the metamaterial sample is absent, the locations of two antennas become indiscernible from the near-field distribution of the electric fields outside the reactive zone ($y > 20$ mm $\sim 0.2\lambda$), as shown in Figs. 3(a) and 3(b). Similarly, from the far-field pattern in Fig. 3(c), one can only find a single lobe. The accurate position of the two sources is difficult to be reconstructed unambiguously from such far-field data, as predicted by the diffraction theory.

We now proceed to insert the nonlinear metamaterial sample 5 mm from the sources ($y = 0.05\lambda$), where the fundamental fields are dominantly evanescent and carry subwavelength spatial information. The generated second harmonic fields at 6 GHz are mapped in the near field and the far field as shown in Figs. 3(d)–3(f). The near-field intensity distribution [Fig. 3(d)] agrees well with the analytical results [Fig. 1(b)] discussed earlier. Compared with the control at the fundamental frequency, the existence of two antenna can be clearly discerned from the near-field distribution [Fig. 3(d) and 3(e)], even at a distance of $y = 40$ mm. Such a distance is far beyond the reactive zone that has been reduced in half as the wavelength of the second harmonic is only one half of the wavelength of the fundamental. The far-field pattern in Fig. 3(f) now exhibits three lobes, drastically different from the case

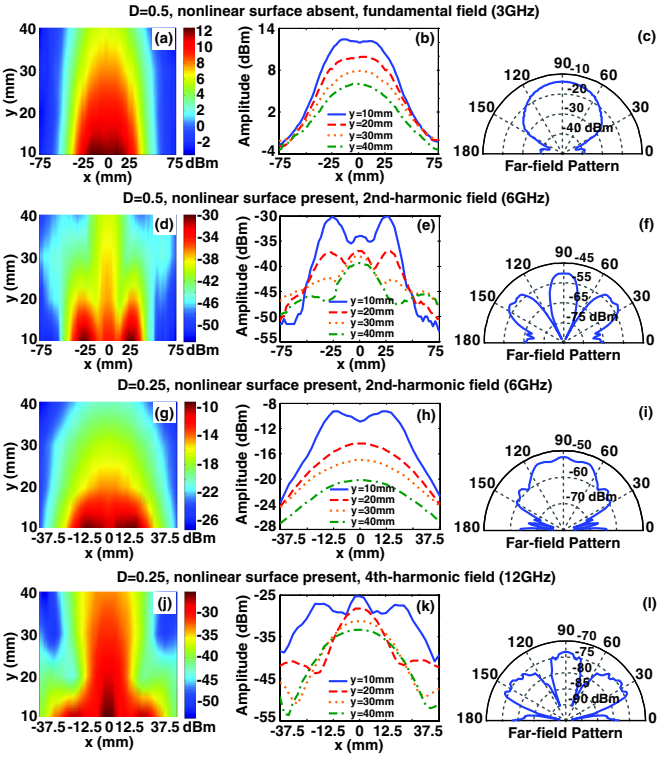

FIG. 3 (color online). Measured near-field and far-field intensity patterns before and after the insertion of the nonlinear surface.

of two indiscernible antennas in Fig. 3(c). A far-field to near-field transformation can then be conducted to recover the individual location of the two antennas.

Since the metamaterial surface exhibits higher order nonlinear response with excellent signal-to-noise ratio, we further extend the harmonic image reconstruction scheme to the fourth harmonic, which, in principle, would result in the spatial resolution being quadrupled. Keeping the experimental conditions unchanged, we reduced the antenna spacing D to 25 mm ($\lambda/4$ for the fundamental). For the second harmonic frequency, such a distance is smaller than the diffraction limit and one can expect that two antennas become once again indiscernible. The measured near-field and far-field patterns at the second-harmonic frequency are shown in Figs. 3(g)–3(i). Both the near-field distribution and far-field pattern revert to the diffraction-limited shapes shown in Figs. 3(a)–3(c), and consequently the two antennas are not spatially resolved beyond the reactive zone. At the fourth harmonic frequency at 12 GHz, on the other hand, the near-field and the far-field distributions [Figs. 3(j)–3(l)] again display interference patterns that allow the locations of the two antennas to be discerned individually.

To recover the image at the source plane from the far-field pattern at harmonic frequencies, one can apply antenna theory (or similarly Fraunhofer diffraction theory in optics) to calculate the source field distribution by

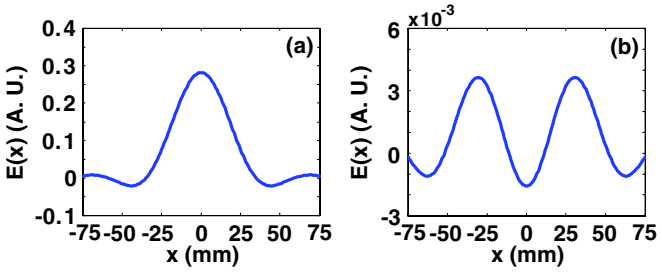

FIG. 4 (color online). Source-plane field distribution derived from: (a) measurement at 3 GHz in the absence of the nonlinear metamaterial surface and (b) measurement at 6 GHz in the presence of the nonlinear metamaterial surface.

performing an inverse Fourier transformation to its far-field pattern [27]. Specifically, we calculate the electric field distribution $E(x)$ at the plane $y = 0$ using the following normalization:

$$E(x) = \int_0^{\pi} E(\varphi) e^{-j2\pi x \cos\varphi/\lambda_m} d\varphi, \tag{2}$$

where $E(\varphi)$ is the angular-dependent far-field pattern, φ is the azimuth angle, and λ_m is the wavelength at which the far-field pattern is measured. Applying Eq. (2) to the E fields derived from the far-field patterns in Figs. 3(c) and 3(f), we obtain the field distribution (image) of the source antennas, as shown in Figs. 4(a) and 4(b), respectively. Although the phase is not directly measured from the spectrum analyzer, the side lobes in both cases are treated to be negative valued, given that the pattern is generated by two linear antennas [27]. In the absence of the metamaterial surface [Fig. 4(a)], the image implies only a single source, whereas with the metamaterial sample [Fig. 4(b)] the image clearly illustrates two discrete sources with $D = 61.5$ mm. The 20% error in the locations of the antenna is due to the phase of the far-field pattern taken to be either 0° or 180°, and more accurate phase measurement is expected to further improve the accuracy of the image [28].

In conclusion, we demonstrate experimentally a nonlinear metamaterial surface that exhibits strong harmonic generation up to the fourth order at low incident power. The artificial nonlinearity could, in principle, be scaled to the entire operational frequency range of microwave diodes, up to few THz [29]. The strong nonlinearity at a moderate power level allows harmonic image reconstruction of samples without nonlinear response. A thin layer of the nonlinear metamaterial placed near the sample has shown enhanced spatial resolutions commensurate with the order of the harmonic generation through inverse Fourier transform of the measured far-field pattern.

Z. Wang is grateful for the generous support and encouragement of M. Soljačić, Y. Fink, and J. D. Joannopoulos. This work is sponsored by the NSFC (No. 61071063 and 60531020), 863 Project (No. 2009AA01Z227), the NCET-07-0750, and the SAEDS project supported by the Ministry of Education.

*Corresponding author: zhwang@MIT.EDU
†Corresponding author: huangfujt@zju.edu.cn
‡Corresponding author: ranlx@zju.edu.cn

[1] J. W. Goodman, *Introduction to Fourier Optics* (McGraw-Hill, New York, 1996), 2nd ed., Chap. 6.5.
[2] J. B. Pendry, Phys. Rev. Lett. **85**, 3966 (2000).
[3] N. Fang *et al.*, Science **308**, 534 (2005).
[4] T. Taubner *et al.*, Science **313**, 1595 (2006).
[5] I. I. Smolyaninov *et al.*, Science **315**, 1699 (2007).
[6] Z. Jacob *et al.*, Opt. Express **14**, 8247 (2006).
[7] A. Salandrino and N. Engheta, Phys. Rev. B **74**, 075103 (2006).
[8] Z. Liu *et al.*, Science **315**, 1686 (2007).
[9] J. Shin, J. T. Shen, and S. Fan, Phys. Rev. B **76**, 113101 (2007).
[10] Z. Dong *et al.*, Appl. Phys. Lett. **96**, 044104 (2010).
[11] D. J. Taatjes and B. T. Mossman, *Cell Imaging Techniques* (Humana Press, Totowa, 2006), 1st ed., Chap. 2.
[12] S. W. Hell, Science **316**, 1153 (2007).
[13] J. T. Bushberg, *The Essential Physics of Medical Imaging* (Lippincott Williams & Wilkins, Philadelphia, 2002), 2nd ed., Chap. 16.
[14] R. W. Boyd, *Nonlinear Optics* (Academic, New York, 2008), 3rd ed..
[15] C. A. Balanis, *Antenna Theory: Analysis and Design* (John Wiley & Sons, New York, 2005), 3rd ed., Chap. 4.4.
[16] J. B. Pendry *et al.*, IEEE Trans. Microwave Theory Tech. **47**, 2075 (1999).
[17] M. W. Klein *et al.*, Science **313**, 502 (2006).
[18] A. A. Zharov, I. V. Shadrivov, and Y. S. Kivshar, Phys. Rev. Lett. **91**, 037401 (2003).
[19] M. Lapine, M. Gorkunov, and K. H. Ringhofer, Phys. Rev. E **67**, 065601 (2003).
[20] M. Gorkunov and M. Lapine, Phys. Rev. B **70**, 235109 (2004).
[21] I. V. Shadrivov *et al.*, Opt. Express **14**, 9344 (2006).
[22] D. A. Powell *et al.*, Appl. Phys. Lett. **91**, 144107 (2007).
[23] I. V. Shadrivov *et al.*, Appl. Phys. Lett. **93**, 161903 (2008).
[24] I. V. Shadrivov *et al.*, Opt. Express **16**, 20266 (2008).
[25] Z. Wang *et al.*, Appl. Phys. Lett. **94**, 134102 (2009).
[26] See the supplemental material at http://link.aps.org/supplemental/10.1103/PhysRevLett.106.047402 for a detailed analysis about retrieving the effective nonlinear coefficient of the nonlinear metamaterial sample.
[27] J. D. Kraus and R. J. Marhefka, *Antennas: For All Applications* (McGraw-Hill, New York, 2003), 3rd ed., Chap. 15.2.
[28] C. Barsi *et al.*, Nat. Photon. **3**, 211 (2009).
[29] T. Suzuki *et al.*, IEEE Trans. Microwave Theory Tech. **47**, 1649 (1999).